Finite spinon density of states in triangular lattice delafossite TlYbSe2

Bishnu P. Belbase, Arjun Unnikrishnan, Shi Feng, Eun Sang Choi, Johannes Knolle, Arnab Banerjee

Angaben zur Veröffentlichung / Publication details:

Belbase, Bishnu P., Arjun Unnikrishnan, Shi Feng, Eun Sang Choi, Johannes Knolle, and Arnab Banerjee. 2026. "Finite spinon density of states in triangular lattice delafossite TlYbSe2." *Physical Review Research* 8 (3): L032021. https://doi.org/10.1103/tc4h-cq9c.

Letter

Finite spinon density of states in triangular lattice delafossite $TlYbSe_2$

Bishnu P. Belbase [1,*] Arjun Unnikrishnan [1,2,*,†,‡] Shi Feng [3,4] Eun Sang Choi [5]
Johannes Knolle [3,4,6] and Arnab Banerjee [1,§]

[1]*Department of Physics and Astronomy, Purdue University, West Lafayette, Indiana 47907, USA*
[2]*Solid State and Structural Chemistry Unit (SSCU), Indian Institute of Science, Bengaluru 560012, India*
[3]*Technical University of Munich, TUM School of Natural Sciences, Physics Department, Garching, Germany*
[4]*Munich Center for Quantum Science and Technology (MCQST), Schellingstraße 4, 80799 München, Germany*
[5]*National High Magnetic Field Laboratory, Tallahassee, Florida 32310, USA*
[6]*Blackett Laboratory, Imperial College London, London SW7 2AZ, United Kingdom*

(Received 9 September 2025; revised 16 December 2025; accepted 8 July 2026; published 11 August 2026)

We introduce the rare-earth delafossite compound $TlYbSe_2$—extending the search for quantum spin liquids in frustrated triangular lattice magnets. While the dc magnetization suggests magnetic exchange interactions on the order of several kelvin, the zero-field ac magnetization and heat capacity measurements reveal no signs of long-range magnetic order down to 20 mK, indicating a quantum-disordered ground state. We observe a spin-freezing transition near ∼30 mK at zero field that is suppressed by an applied magnetic field of ∼0.02 T. A broad anomaly in the heat capacity measurements between 2 and 5 K is indicative of short-range spin correlations. Below 350 mK, we observe a robust linear temperature dependence of the heat capacity, accompanied by the complete absence of long-range order at low fields. We propose that a phenomenological theory, based on the interplay between spinons and thermally excited gauge flux excitations, can account for the linear temperature dependence of the heat capacity, and could be widely applicable to similar critical quantum spin liquid candidate materials. The results establish the low-temperature, low-field regime of $TlYbSe_2$ as a prime candidate for field-tunable triangular quantum spin liquid behavior and highlight the importance of thermally excited gauge field excitations.

DOI: 10.1103/tc4h-cq9c

Introduction. Quantum spin liquids (QSLs) are exotic states of matter sought after in low-dimensional frustrated magnets with potential applications ranging from quantum memory to topologically protected qubits [1–16]. The two-dimensional (2D) triangular lattice stands out as Anderson's original proposal for a simple QSL platform [2,17–19], promising a variety of interesting states. However, proving such a QSL ground state experimentally is a challenging task [3,20]. While the absence of long-range order (LRO) down to subkelvin temperatures often hints at QSL behavior, alternative scenarios—such as disorder [21], spin glass [22], random singlet phases [23], eminuscent phases [24], or ultralow-temperature ordering [25]—complicate definitive identification. Thus, a comprehensive set of bulk measurements is essential to disentangle these possibilities and establish the true nature of the ground state.

Recently, the rare-earth triangular lattice compounds have gained attention [20,28–39]. Especially, the Yb^{3+}-based delafossites ($AYbX_2$, with A = monovalent cation; X = O, S, Se, or Te) offer an ideal 2D triangular lattice geometry of effective spin-1/2 states of Yb^{3+} ions. These systems offer tunable interlayer and intralayer interactions via A- or X-site substitution [40,41]. Recently, some candidates of the family $AYbX_2$ have already been shown to exhibit proximate QSL phases [9,30–35,42–48]. Interestingly, $NaYbSe_2$ and $KYbSe_2$ have exhibited signatures of proximity to the quantum critical point (QCP) separating the LRO from QSL phases, as fine-tuning the A-site cation enables control over the J_2/J_1 ratio [26,27].

In this work, we explore $TlYbSe_2$, a recent member of the delafossite family where thallium, a non-alkali metal, occupies the A site [49], and establish it as a prime QSL candidate. We report the millikelvin temperature thermodynamic and magnetic properties of $TlYbSe_2$ using dc/ac magnetization and heat capacity measurements down to 20 mK. We find no evidence of magnetic LRO down to the lowest temperature. Both the heat capacity studies and the lattice constants place this compound between $NaYbSe_2$ and $KYbSe_2$ in the J_2/J_1 phase diagram [Fig. 1(d)] near the QCP leading to the QSL phase, where quantum fluctuations are strongest. We observe a frequency-dependent spin-freezing anomaly near 30 mK, an effect not previously explored in any member of this family. Importantly, we find that the magnetic heat capacity exhibits a robust linear-in-T dependence below 350 mK.

*These authors contributed equally to this work.
†Contact author: arjunpookad@gmail.com
‡Present address: Experimental Physics VI, Center for Electronic Correlations and Magnetism, Institute of Physics, University of Augsburg, Augsburg 86159, Germany.
§Contact author: arnabb@purdue.edu

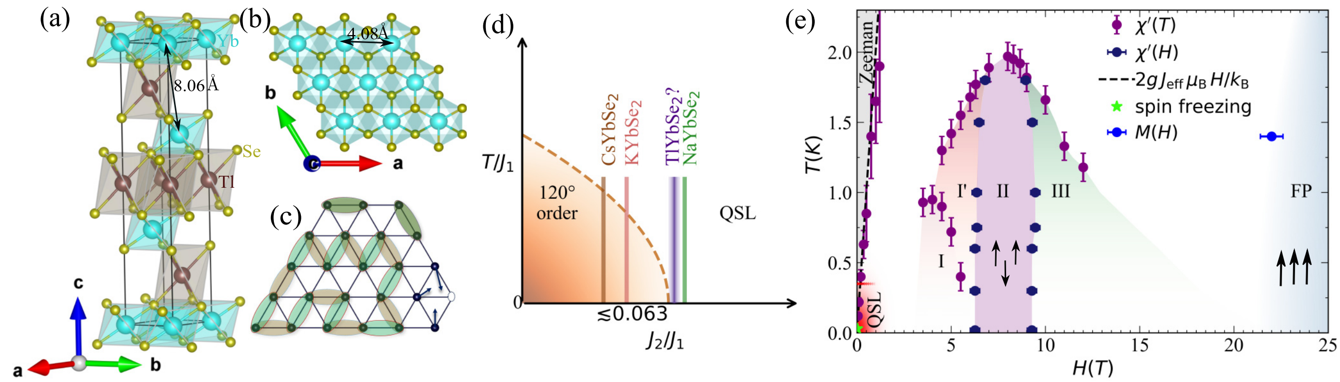

FIG. 1. Crystal structure and phase diagram. (a) Crystal structure of $TlYbSe_2$, showing the stacking of Yb triangular layers separated by Tl layers along the *c* axis. (b) Top view of the Yb triangular lattice in the *ab* plane, where magnetic interactions are mediated by edge-sharing $YbSe_6$ octahedra. (c) A schematic representation highlighting the coexistence of a resonating valence bond state with possible localized spin freezing in a triangular lattice geometry. (d) Phase diagram showing the position of $TlYbSe_2$ in comparison to other triangular lattice compounds in the $AYbSe_2$ family. The phase diagram and position of other compounds are adapted from Refs. [26,27]. The QCP at $J_2/J_1 \lesssim 0.063$ separates the 120° ordered state and the QSL regime. The position of $TlYbSe_2$ is estimated from our experimental observations and lies near the QCP. (e) Temperature-field (H-T) phase diagram of $TlYbSe_2$ based on anomalies in the real part of the ac susceptibility [$\chi'(T)$ (purple) and $\chi'(H)$ (dark blue)], magnetization $M(H)$, and heat capacity $C_p(T)$. The black dashed line indicates Zeeman-driven quenching of free Yb moments. The green star denotes a low-temperature spin-freezing anomaly. The horizontal red dotted line, extracted from zero-field $C_p(T)$, indicates the crossover into the proposed QSL regime, highlighted in red at low fields and temperatures. Field-induced magnetic phases are labeled as I, I′, II, and III, with FP denoting the field-polarized state.

This *linear* heat capacity, also observed earlier in isostructural $NaYbSe_2$ [31,44], remained a conundrum because the theoretically expected QSL ground state for the J_1-J_2 Heisenberg model on the triangular lattice is a critical Dirac QSL [19,50–52], which is characterized by a *quadratic* temperature dependence of the specific heat. This expectation stems from the density of states (DOS) vanishing linearly in energy for the critical Dirac QSL, i.e., most simply arising from a Dirac spectrum of fermionic spinons in a fixed translationally invariant gauge flux background. However, at any nonzero temperature, our phenomenological theory shows that the gauge flux excitations proliferate, thereby acting as self-generated disorder, leading to a nonvanishing spinon DOS. Thus, we reconcile a DSL ground state with a linear-in-temperature heat capacity measured experimentally not only here for $TlYbSe_2$, but also for many other QSL candidate materials [18].

Compound and thermodynamic measurements. $TlYbSe_2$ crystallizes in a delafossite-type structure with a trigonal $R\bar{3}m$ (No. 166) space group. The structure consists of 2D triangular layers of edge-sharing, distorted $YbSe_6$ octahedra in the *ab* plane, separated by $TlSe_6$ layers [Figs. 1(a) and 1(b)]. The Yb-Yb distance in a triangular layer is ∼4.08 Å. The unit cell contains three $YbSe_6$ layers stacked along the *c* axis, with an interlayer Yb-Yb distance of ∼8.06 Å. Due to the larger ionic radius of Tl^+, the interlayer Yb-Yb spacing in $TlYbSe_2$ is notably larger than that in most well-studied delafossites—such as $NaYbSe_2$ (∼7.3 Å), $NaYbO_2$ (∼5.85 Å), and $KYbSe_2$ (∼7.93 Å) [30,31,33]. This increased spacing is expected to weaken interlayer magnetic coupling, enhance two-dimensionality, and strengthen quantum fluctuations—conditions that may favor the emergence of a QSL ground state.

To investigate the nature and strength of the magnetic exchange interactions, we performed dc magnetization measurements (see the Supplemental Material [53] for experimental details, which includes Refs. [19,27,29,31,33,52,54–68]). The inverse magnetic susceptibility, $1/\chi(T)$, measured under an applied magnetic field of 0.5 T [Fig. 2(a)], shows a linear behavior above 150 K, which can be described by the modified Curie-Weiss (CW) law (see the Supplemental Material [53]). The deviation from linear behavior below 100 K suggests thermal depopulation of excited crystalline electric field (CEF) levels. A low-T CW fit below 5 K yields T-independent susceptibility $\chi_0 \simeq 6.9 \times 10^{-3}$ emu/(mol Oe), effective moment $\mu_{\rm eff}^{\rm LT} \simeq 2.6\mu_B$, CW temperature $\theta_{\rm CW}^{\rm LT} \simeq -13.8$ K, and a Landé g factor $g \simeq 3.0$, consistent with a Kramers doublet $J_{\rm eff} = 1/2$ ground state. The large negative $\theta_{\rm CW}^{\rm LT}$ indicates dominant antiferromagnetic (AFM) exchange, with the nearest-neighbor exchange coupling estimated as $J_1 \simeq 9.2$ K using $\theta_{\rm CW} = -3J_1/2$ [46,69]. Notably, the values of $\theta_{\rm CW}$ and J_1 for $TlYbSe_2$ are much higher than those of its isostructural counterparts [31,33,34,46], indicating stronger AFM exchange interactions.

The isothermal magnetization $M(H)$ measured at 1.4 K [Fig. 2(b)] saturates near $H_{\rm sat} \simeq 22$ T, indicating strong AFM coupling. A finite slope beyond saturation reflects Van Vleck contributions, typical for Yb^{3+} systems. A linear fit in the high-field range (32–35 T) yields a saturation moment $M_{\rm sat} \simeq 1.4\mu_B$, consistent with a $J_{\rm eff} = 1/2$ ground state and $g \simeq 2.8$. Using the relation $\mu_0 H_{\rm sat} = 9J_{\rm eff}J_1k_B/\mu_B g$, the exchange coupling is estimated as $J_1 \simeq 9.2$ K, in excellent agreement with the value from the low-T CW analysis. The plateau near $M_{\rm sat}/3$ corresponds to the up-up-down (UUD) spin configuration—a hallmark of triangular lattice antiferromagnets (TLAFs) [2,70–72].

To further understand the low-T magnetism and field effects in $TlYbSe_2$, we performed ac susceptibility measurements (see the Supplemental Material [53]). The real part, $\chi'(T)$, measured at 137 Hz under zero field, ex-

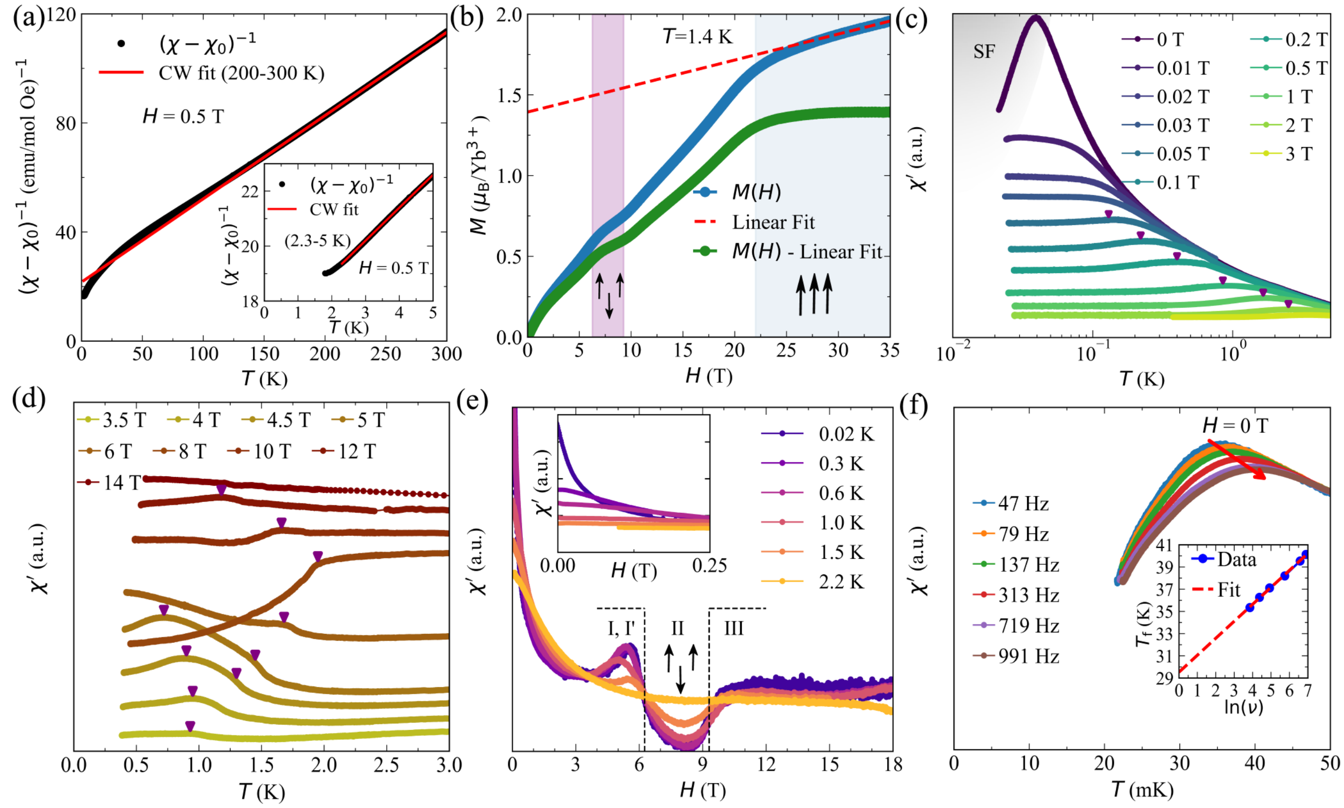

FIG. 2. Ac and dc magnetization. (a) Temperature-dependent inverse dc magnetic susceptibility ($1/\chi(T)$) at 0.5 T, with a modified CW fit in the high-T region. Inset: Low-T CW fit. (b) Isothermal magnetization $M(H)$ measured at 1.4 K, showing saturation near $H_{\rm sat} \simeq 22$ T. The red dashed line represents a linear fit in the high-field region, yielding $M_{\rm sat} \simeq 1.4\mu_B$ per Yb^{3+}. The green curve represents the magnetization after subtracting the linear high-field slope from the raw $M(H)$ data. A magnetization plateau near $M_{\rm sat}/3$, characteristic of the up-up-down configuration in triangular lattice antiferromagnets, is clearly visible. (c) Real part of ac susceptibility $\chi'(T)$ at low fields (0–3 T); purple arrows mark broad maxima due to Zeeman splitting. The light gray-shaded region marks the spin-freezing regime. (d) $\chi'(T)$ at high fields (3.5–14 T), where the system is in a magnetically ordered state. Curves are vertically offset for clarity (nonuniformly); original plots with no vertical offset data are provided in the Supplemental Material [53]. Purple arrows mark transition temperatures. (e) Field-dependent $\chi'(H)$ data measured at various temperatures, with phase boundaries denoted by dotted black lines. The inset highlights the low-field behavior, showing a rapid suppression of χ' with increasing temperature. (f) $\chi'(T)$ measured at different frequencies in the 20–50 mK range at zero field reveals a frequency-dependent spin-freezing anomaly (y axis starts at origin). The red arrow marks the shift in the freezing temperature ($T_{\rm f}$) with frequency (ν). Inset: $T_{\rm f}$ vs $\ln(\nu)$, with a linear fit shown by the red dashed line.

hibits a sharp peak around ∼37 mK [Fig. 2(c)], which shifts to higher temperatures with increasing frequency (ν) [Fig. 2(f)]—a hallmark of spin freezing. An empirical linear extrapolation of $\ln(\nu)$ versus freezing temperature ($T_{\rm f}$) to 1 Hz yields a spin-freezing transition temperature of 29.5(2) mK [Fig. 2(f), inset]. The corresponding Mydosh parameter [73,74], $\delta T_{\rm f} = \Delta T_{\rm f}/T_{\rm f}\Delta\log_{10}(\nu) > 0.1$, is considerably larger than the values typically reported for canonical spin glasses (∼0.005–0.01) and cluster glasses [74,75], consistent with spin freezing associated with weakly interacting or nearly noninteracting magnetic entities rather than a conventional spin-glass state. Applying a small magnetic field of ∼0.02 T suppresses the zero-field peak in $\chi'(T)$, consistent with the energy (temperature) scale of the spin-freezing transition.

Upon further increasing field, a broad maximum appears [Fig. 2(c)] that shifts linearly, consistent with Zeeman splitting $\Delta E = 2\mu_B g J_{\rm eff} H$ of isolated Yb^{3+} ($J_{\rm eff} = 1/2$) moments, such as those at grain boundaries of the polycrystalline sample. This aligns with the $M(H)$ data at 1.8 K, indicating that ∼3% of the moments remain as free spins (see the Supplemental Material [53]). A similar behavior was reported in $NaYbO_2$ with ∼7% free spins [33]. With increasing magnetic field beyond 3.5 T, $TlYbSe_2$ enters a magnetically ordered state [Fig. 2(d)]. The ac susceptibility signal decreased with increasing dc field, as the dc field acts as a bias that aligns magnetic moments and thereby suppresses their response to the small oscillating ac field [76]. As a result, anomalies in $\chi'(T)$ above 12 T lie beyond the resolution. The $\chi'(H)$ curves at different temperatures [Fig. 2(e)] cross near ∼3.5 T, where the system enters into an ordered state, followed by a peak at ∼5.5 T and a dip at ∼8 T—corresponding to the $M_{\rm sat}/3$ plateau in $M(H)$ [Fig. 2(b)]. Beyond 8 T, $\chi'(H)$ recovers, marking a high-field boundary.

The temperature-field (H-T) phase diagram constructed from $\chi'(T)$, $\chi'(H)$, and $M(H)$ measurements is shown in Fig. 1(e). As the magnetic field increases, the system enters a field-induced magnetic LRO regime comprising multiple distinct phases. At low fields, the system transitions through phases I and I′, followed by phase II, centered around 6.3–

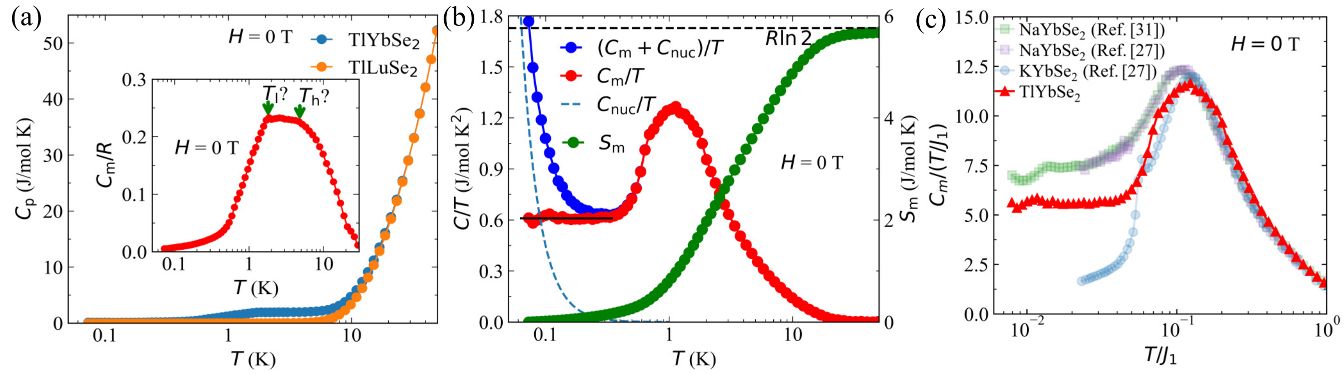

FIG. 3. Specific heat capacity. (a) Zero-field specific heat, $C_p(T)$, of $TlYbSe_2$ measured down to 70 mK, overlaid with the phonon contribution $C_{ph}(T)$ from nonmagnetic $TlLuSe_2$. Inset: Magnetic heat capacity C_m/R showing two broad maxima near $T_l \simeq 2$ K and $T_h \simeq 5$ K. (b) Zero-field heat capacity after subtracting $C_{ph}(T)$: C/T vs T (left y axis) and magnetic entropy S_m vs T (right y axis). The solid black line on C_m/T serves as a guide to the eye and indicates low-T linearity. The dotted line marks $R\ln 2$ (right y axis). (c) Comparison of the magnetic specific heat C_m of $TlYbSe_2$ with $KYbSe_2$ and $NaYbSe_2$, plotted as $C_m/(T/J_1)$ vs (T/J_1). The $KYbSe_2$ data are adapted from Ref. [27], while the $NaYbSe_2$ data are adapted from Refs. [27,31]. $TlYbSe_2$ lies between the two at low T and shows a pronounced linear component.

9.3 T, and then into phase III, which extends up to the saturation field of ∼22 T. Phases I and I′ likely correspond to 120° or oblique (Y-coplanar) spin structures, and phase II is attributed to the UUD configuration, as evidenced by the suppression of $\chi'(H)$ [Fig. 2(e)] and the magnetization plateau at $M_{sat}/3$ [Fig. 2(b)]. Phase III has been proposed to correspond to a 2 : 1 canted phase [77].

To investigate the nature of the quantum disordered ground state in $TlYbSe_2$, we measured the zero-field specific heat $C_p(T)$ down to 70 mK [Fig. 3(a)], along with that of the nonmagnetic analog $TlLuSe_2$ to estimate the phonon background $C_{ph}(T)$. The magnetic contribution, $C_m(T)$, was obtained by subtracting $C_{ph}(T)$ and the low-T nuclear Schottky term $C_{nuc}(T)$, extracted via fitting (discussed below). The $C_m(T)$ shows no sign of magnetic LRO, consistent with ac susceptibility results. Instead, a broad maximum is observed between 2 and 5 K [inset, Fig. 3(a)], characteristic of low-dimensional frustrated systems and indicative of a crossover into a QSL regime [57,78].

Notably, related compounds such as $NaYbO_2$ and $NaYbSe_2$ exhibit similar broad maxima arising from a superposition of two broad peaks, suggesting two distinct exchange energy scales [31,33]. Such double maxima in $C_p(T)$ have been theoretically predicted for 2D triangular and kagome antiferromagnets with fully frustrated disordered ground states [79,80] and observed experimentally in several TLAF systems [31,33,81,82]. For spin-1/2 TLAFs, the two crossover temperatures are expected at $T_l/J = 0.2$ and $T_h/J = 0.55$ [83]. With $J \simeq 9.2$ K, the observed maxima in $TlYbSe_2$ fall near these theoretical values. The peak value $C_m^{max} \simeq 0.23R$ also agrees with predictions for fully frustrated TLAFs [84,85].

The zero-field C/T after subtracting the phonon part is shown in Fig. 3(b) (left y axis). Below 300 mK, an upturn appears due to a nuclear Schottky contribution—typical for Yb-based systems [31,86]. The low-T data ($T < 350$ mK) were fitted using $C(T) = \alpha/T^2 + \gamma T^b$, where the first term captures the nuclear Schottky contribution (C_{nuc}) and the second term reflects the intrinsic magnetic part (C_m). The fit yields $\alpha = 4.468(75) \times 10^{-4}$ J K/mol, $\gamma = 0.62(1)$ J/(mol K^2), and $b = 1.01(1)$. For a $U(1)$ Dirac spin liquid, the magnetic heat capacity is expected to follow a T^2 dependence. However, a pure T^2 fit fails to describe the observed behavior [see Fig. S4(c) in the Supplemental Material [53]]. The magnetic entropy S_m, obtained by integrating C_m/T from 70 mK, recovers ∼98% of $R\ln 2$ by 20 K [Fig. 3(b)], suggesting a Kramers doublet ground state with effective spin 1/2 for Yb^{3+}. Additionally, only 2% of the total magnetic entropy remains below 70 mK, which provides a bound to the maximum entropy released at the spin-freezing regime.

Interestingly, the low-T magnetic heat capacity of $TlYbSe_2$ lies between those of $KYbSe_2$ and $NaYbSe_2$ [27], as shown in Fig. 3(c), placing it between the two in the J_2/J_1 phase diagram [Fig. 1(d)]. Using $J_1 = 9.2$ K, this provides an initial estimate of J_2 between 0.58 and 0.64 meV. Combined with the absence of 120° magnetic order in the low-field regime below 2 T and down to 20 mK, these findings suggest that $TlYbSe_2$ lies closer to the QCP than other delafossite candidates. This trend in heat capacity faithfully reflects the distances Yb-Yb within the triangular layer, which increase from 4.06 Å in $NaYbSe_2$ to 4.08 Å in $TlYbSe_2$, 4.11 Å in $KYbSe_2$, and 4.15 Å in $CsYbSe_2$. This structural trend further supports the placement of $TlYbSe_2$ in the phase diagram and highlights Yb-Yb spacing as a useful indicator for bulk thermodynamic behavior and proximity to a QSL state. Notably, the key results presented here—such as the observation of spin freezing at ultralow temperatures and linear-in-T specific heat—were obtained under zero field, meaning they are independent of the crystallographic field direction. As such, measurements on polycrystalline and single-crystalline samples are expected to yield similar results.

Thermal flux proliferation. The near-linear T dependence ($b \simeq 1$) of magnetic specific heat $C_m(T)$, along with the absence of magnetic LRO down to 20 mK, suggests a nonvanishing DOS at low energy in the QSL phase [5]. Such linear-in-T specific heat arises naturally in a QSL with a spinon Fermi surface, but no microscopic models and mechanisms are known that stabilize a spinon Fermi surface state

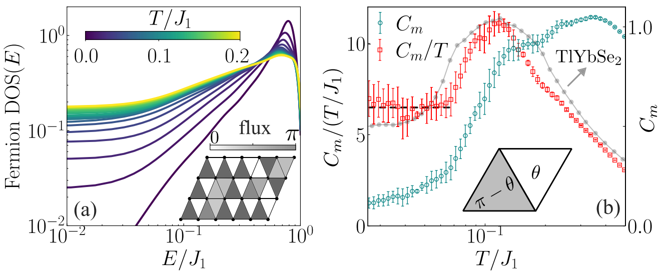

FIG. 4. Results from the phenomenological theory. (a) Fermionic spinon DOS as a function of temperature. The temperature sets the density of excited gauge fluxes; see inset for an illustration of a flux configuration. (b) Rescaled magnetic specific heat presented as C_m/T (red box, left axis) and C_m (teal box, right axis) from importance sampling for the effective theory, overlaid on the C_m/T data measured from $TlYbSe_2$ (gray dots, left axis). The horizontal dashed line is the eye-guiding line emphasizing the constant C_m/T from the theory. The inset shows a local flux variation with phase angle θ on top of the staggered flux configurations of the ground-state Dirac QSL.

on the triangular lattice [19]. In the following, we show how thermally excited fluxes at finite energy scales above a $U(1)$ Dirac QSL ground state can generate a *finite* spinon DOS at low energy inducing a linear $C_\mathrm{m}(T)$. We note that our proposed mechanism is the $U(1)$ analog of the enhancement in low-energy DOS produced by fluctuating Z_2 fluxes in the Kitaev spin liquid [65–67,87,88]. There, the low-energy spinon DOS emerges similarly from the thermal proliferation of local fluxes.

Following the standard parton mean-field theory, we assume that the fermionic spinons propagate in a staggered π-flux background, corresponding to $J_2/J_1 \sim \frac{1}{8}$ with Dirac spinons at ultralow energy scales [19]. We assume a separation of scale such that the dynamics of the background gauge field excitations are decoupled from the spinons—The latter see a given gauge field configuration as a static background flux. This can be described by an effective Hamiltonian $H = \sum_i E_M^i(F)\, a_i^\dagger a_i + \sum_{\theta\in[0,2\pi)} \sum_m \Delta(\theta) (f_m^\theta)^\dagger f_m^\theta$, where $a_i^\dagger$ create matter fermions with energy $E_M^i(F)$ in a given flux background F and $(f_m^\theta)^\dagger$ create a local $U(1)$ flux excitation with a phase angle θ and gap $\Delta(\theta)$ [see insets of Figs. 4(a) and 4(b)]. Note that because of the $U(1)$ nature of the gauge field local flux excitations are gapless in contrast to the Kitaev Z_2 case. We can then perform importance sampling of the joint flux-fermion distribution. We find that the fermion DOS, which vanishes linear in energy at zero temperature without local flux excitations, becomes finite once thermal fluxes proliferate under finite T [Fig. 4(a)]. Immediately above the temperature scale $T/J_1 \sim 10^{-2}$ at which this DOS becomes a finite constant, the specific heat capacity follows $C_m \propto T$ [Fig. 4(b)], and even quantitatively matches the linear specific heat observed experimentally in Fig. 3, albeit with a minor shift in the linear-T plateau possibly stemming from the Schottky-peak subtraction partially removing the flux contribution. Indeed, the overall match of the theoretical C_m/T with the experimental data for $J \simeq 9.2$ K and the amplitude as the only free parameter is remarkable [Fig. 4(b)]. Thus, the finite-T thermodynamics of a zero-temperature $U(1)$ Dirac spin liquid can be fully consistent with our data; details of the phenomenological model are given in the Supplemental Material [53].

Discussion. The powder results presented here are dominated by grains aligned with the *ab*plane—statistically responsible for roughly two-thirds of the contribution. Also, a strong magnetic anisotropy in delafossites typically causes features associated with $H||c$ to appear only at very high fields, likely beyond the field range accessed in this study [31]. As a result, even though our measurements were performed on polycrystalline samples with randomly oriented grains, the field-induced transitions remain sharp—comparable to those seen in single crystals. Consequently, the use of polycrystalline samples does not compromise the accuracy of the phase diagram, which closely resembles those reported for related delafossites under *ab*-plane magnetic fields [31,89]. Importantly, the linear-in-T trend of the low-temperature magnetic heat capacity is observed in zero-field measurement, making it independent of field orientation and therefore unaffected by whether the sample is single crystalline or polycrystalline.

It is natural to question whether the linear γT term can simply arise from the estimated 3% free-spin population. If we assume that all of the observed linear γT contribution originates from these free spins, the measured $\gamma = 0.62$ J/(mol K^2) over the range 0.07–0.35 K consumes essentially the full $0.03\,R\ln 2$ entropy available from a 3% free-spin fraction. Any free-spin-driven freezing at 0.03 K would also need to draw from this same finite entropy budget, leaving the free-spin-only explanation internally inconsistent. Furthermore, a free-spin-generated linear term could naturally extend from the spin-freezing scale (∼30 mK) up to the magnetic energy scale $|J| \approx 9.2$ K, which would imply an entropy release of ∼5.7 J/(mol K), comparable to the full spin entropy $R\ln 2$ and nearly 30 times larger than the 0.173 J/(mol K) available from the estimated free-spin population. Conversely, a realistic free-spin contribution to a linear term over this range would be limited to $0.173/(9.2 - 0.03) \simeq 0.02$ J/(mol K^2), far smaller than the measured γ. Moreover, a true γT term is characteristic of intrinsic gapless excitations, whereas dilute free-spin or defect contributions typically produce nonlinear specific heat that only mimics linearity over a narrow window unless the associated energy scales are extremely fine-tuned [90]. Overall, the linear γT term appears to be a standard observable of delafossites in the spin-liquid regime; the excellent agreement of our data with the phenomenological theory—including the Schottky anomaly—therefore provides a far more natural explanation.

We have shown that this linear behavior is consistent with a finite low-energy spinon DOS, which is borne out from the thermal proliferation of flux excitations of a $U(1)$ Dirac QSL. Our result establishes linear behavior of the heat capacity not only as a general feature of delafossites but also as a defining signature of Dirac QSL physics with thermally excited fluxes. Comparative analysis of heat capacity data places $TlYbSe_2$ between $NaYbSe_2$ and $KYbSe_2$ in the J_2/J_1 phase diagram, suggesting closer proximity to a QCP separating magnetic order from a spin-liquid regime.

The spin freezing below 30 mK marks a new discovery in the delafossites, which has since also been reported in $NaYbSe_2$ and $Cu_{1.14}YbSe_2$ [27,91]. The observation of the spin-freezing transition at ultralow temperatures further calls for future studies of similar spin freezing in other delafossites, and cautions against readily interpreting low-temperature anomalies as spin gaps. The microscopic origin of this spin freezing, however, remains unknown. The possibility of static chemical defects cannot be ruled out [92], arising perhaps from a low density of selenium vacancies where orphan moments produce local pockets of spin freezing, while the remainder of the lattice retains highly fluctuating spins down to zero temperature, similar to a scenario proposed for the Dirac QSL candidate $YbZn_2GaO_5$ [36]. Within the $U(1)$ QSL framework, it is also possible to conjecture an idea of self-generated quantum glassiness in the presence of slow random fluxes, which act like emergent defects. Mobile spinons may localize in the presence of thermally excited flux disorder, akin to the case of the Z_2 Kitaev QSL [87,88]. Establishing such mechanisms quantitatively would be a promising future endeavor requiring careful low-field millikelvin specific-heat and thermal-conductivity measurements and calculating accompanying dynamical observables. Any such theory must also account for the constraints that the transition involves at best ∼2% of the total $R \ln 2$ entropy and is suppressed by a very small magnetic field of approximately 0.02 T.

Overall, our results establish $TlYbSe_2$ as a prime platform for studying triangular lattice QSL physics. Investigating transport properties and dynamical observables within such a scenario for $U(1)$ QSLs will be a promising direction for future studies.

Note added. Curiously, recent measurements of combined thermal transport and specific heat in Na-based delafossite brethren compounds provide evidence for a strong suppression of thermal conductivity interpreted in terms of random entanglement scales related to dimer propagation [44,92]. However, here we hypothesize an alternative intrinsic mechanism: In our picture, fluctuating $U(1)$ fluxes can generate a linear specific heat without requiring strong extrinsic defects, while their slow dynamics act as a quasistatic disorder background for spinons, thereby suppressing the spinon heat transport, providing a consistent explanation. We expect that thermal transport measurements on (partly doped) $TlYbSe_2$ will tease apart these possibilities in the future.

Acknowledgments. We thank A. O. Scheie, D. D. Sarma, and J. Xing for the fruitful discussions and valuable suggestions. B.P.B., A.B., and the research as a whole was supported by the U.S. Department of Energy—Office of Science, Basic Energy Sciences (Grant No. DE-SC0022986), under the project "Seeking quasiparticles in perturbed matter from low-energy spin dynamics". A.U. acknowledges financial support from the Department of Science and Technology (DST), Government of India, through the DST-INSPIRE Faculty Fellowship (Ref. No. DST/INSPIRE/04/2019/001664), as well as from the Quantum Science Center, a National Quantum Initiative Science Research Center funded by the U.S. Department of Energy. S.F. and J.K. acknowledge support from Deutsche Forschungsgemeinschaft (DFG, German Research Foundation) under Germany's Excellence Strategy–EXC–2111–390814868, TRR 360 – 492547816 and DFG Grants No. KN1254/1-2 and No. KN1254/2-1, the Imperial-TUM flagship partnership, the European Research Council (ERC) under the European Union's Horizon 2020 Research and Innovation Programme (Grant Agreement No. 851161), the European Union (Grant Agreement No. 101169765), as well as the Munich Quantum Valley, which is supported by the Bavarian state government with funds from the Hightech Agenda Bayern Plus. Part of this work was conducted at the National High Magnetic Field Laboratory, supported by the National Science Foundation (Cooperative Agreement No. DMR-2128556) and the State of Florida. B.P.B. acknowledges the Quantum Design Winter School, where millikelvin specific heat capacity data were collected.

Data availability. The experimental data supporting the findings of this work have been deposited in the publicly accessible Zenodo repository [93].

[1] E. Dennis, A. Kitaev, A. Landahl, and J. Preskill, Topological quantum memory, J. Math. Phys. **43**, 4452 (2002).

[2] L. Balents, Spin liquids in frustrated magnets, Nature (London) **464**, 199 (2010).

[3] L. Savary and L. Balents, Quantum spin liquids: A review, Rep. Prog. Phys. **80**, 016502 (2017).

[4] J. Knolle and R. Moessner, A field guide to spin liquids, Annu. Rev. Condens. Matter Phys. **10**, 451 (2019).

[5] Y. Zhou, K. Kanoda, and T.-K. Ng, Quantum spin liquid states, Rev. Mod. Phys. **89**, 025003 (2017).

[6] D. Hirobe, M. Sato, T. Kawamata, Y. Shiomi, K.-I. Uchida, R. Iguchi, Y. Koike, S. Maekawa, and E. Saitoh, One-dimensional spinon spin currents, Nat. Phys. **13**, 30 (2017).

[7] C. Broholm, R. Cava, S. Kivelson, D. Nocera, M. Norman, and T. Senthil, Quantum spin liquids, Science **367**, eaay0668 (2020).

[8] Y. Li, G. Chen, W. Tong, L. Pi, J. Liu, Z. Yang, X. Wang, and Q. Zhang, Rare-earth triangular lattice spin liquid: A single-crystal study of $YbMgGaO_4$, Phys. Rev. Lett. **115**, 167203 (2015).

[9] M. M. Bordelon, C. Liu, L. Posthuma, P. Sarte, N. Butch, D. M. Pajerowski, A. Banerjee, L. Balents, and S. D. Wilson, Spin excitations in the frustrated triangular lattice antiferromagnet $NaYbO_2$, Phys. Rev. B **101**, 224427 (2020).

[10] T. Arh, B. Sana, M. Pregelj, P. Khuntia, Z. Jagličić, M. Le, P. Biswas, P. Manuel, L. Mangin-Thro, A. Ozarowski, *et al.*, The Ising triangular-lattice antiferromagnet neodymium heptatantalate as a quantum spin liquid candidate, Nat. Mater. **21**, 416 (2022).

[11] Y. Shimizu, K. Miyagawa, K. Kanoda, M. Maesato, and G. Saito, Spin liquid state in an organic Mott insulator with a triangular lattice, Phys. Rev. Lett. **91**, 107001 (2003).

[12] J. Helton, K. Matan, M. Shores, E. Nytko, B. Bartlett, Y. Yoshida, Y. Takano, A. Suslov, Y. Qiu, J.-H. Chung, *et al.*, Spin dynamics of the spin-1/2 kagome lattice antiferromagnet $ZnCu_3(OH)_6Cl_2$, Phys. Rev. Lett. **98**, 107204 (2007).

[13] T.-H. Han, J. S. Helton, S. Chu, D. G. Nocera, J. A. Rodriguez-Rivera, C. Broholm, and Y. S. Lee, Fractionalized excitations in the spin-liquid state of a kagome-lattice antiferromagnet, Nature (London) **492**, 406 (2012).

[14] Z. Feng, Z. Li, X. Meng, W. Yi, Y. Wei, J. Zhang, Y.-C. Wang, W. Jiang, Z. Liu, S. Li, *et al.*, Gapped spin-1/2 spinon excitations in a new kagome quantum spin liquid compound $Cu_3Zn(OH)_6FBr$, Chin. Phys. Lett. **34**, 077502 (2017).

[15] A. Banerjee, C. Bridges, J.-Q. Yan, A. Aczel, L. Li, M. Stone, G. Granroth, M. Lumsden, Y. Yiu, J. Knolle, *et al.*, Proximate Kitaev quantum spin liquid behaviour in a honeycomb magnet, Nat. Mater. **15**, 733 (2016).

[16] Z. Meng, T. Lang, S. Wessel, F. Assaad, and A. Muramatsu, Quantum spin liquid emerging in two-dimensional correlated Dirac fermions, Nature (London) **464**, 847 (2010).

[17] P. W. Anderson, Resonating valence bonds: A new kind of insulator? Mater. Res. Bull. **8**, 153 (1973).

[18] K. Kanoda and R. Kato, Mott physics in organic conductors with triangular lattices, Annu. Rev. Condens. Matter Phys. **2**, 167 (2011).

[19] Y. Iqbal, W.-J. Hu, R. Thomale, D. Poilblanc, and F. Becca, Spin liquid nature in the Heisenberg J_1-J_2 triangular antiferromagnet, Phys. Rev. B **93**, 144411 (2016).

[20] J. Wen, S.-L. Yu, S. Li, W. Yu, and J.-X. Li, Experimental identification of quantum spin liquids, npj Quantum Mater. **4**, 12 (2019).

[21] Z. Zhu, P. Maksimov, S. R. White, and A. Chernyshev, Disorder-induced mimicry of a spin liquid in $YbMgGaO_4$, Phys. Rev. Lett. **119**, 157201 (2017).

[22] M. R. Norman, Colloquium: Herbertsmithite and the search for the quantum spin liquid, Rev. Mod. Phys. **88**, 041002 (2016).

[23] P. Song, K. Zhu, F. Yang, Y. Wei, L. Zhang, H. Yang, X.-L. Sheng, Y. Qi, J. Ni, S. Li, *et al.*, Evidence for the random singlet phase in the honeycomb iridate $SrIr_2O_6$, Phys. Rev. B **103**, L241114 (2021).

[24] S. Syzranov and A. Ramirez, Eminuscent phase in frustrated magnets: A challenge to quantum spin liquids, Nat. Commun. **13**, 2993 (2022).

[25] Y. Tokiwa, S. Bachus, K. Kavita, A. Jesche, A. A. Tsirlin, and P. Gegenwart, Frustrated magnet for adiabatic demagnetization cooling to milli-kelvin temperatures, Commun. Mater. **2**, 42 (2021).

[26] A. Scheie, Y. Kamiya, H. Zhang, S. Lee, A. Woods, M. Ajeesh, M. Gonzalez, B. Bernu, J. Villanova, J. Xing, *et al.*, Nonlinear magnons and exchange Hamiltonians of the delafossite proximate quantum spin liquid candidates $KYbSe_2$ and $NaYbSe_2$, Phys. Rev. B **109**, 014425 (2024).

[27] A. Scheie, M. Lee, K. Wang, P. Laurell, E. Choi, D. Pajerowski, Q. Zhang, J. Ma, H. Zhou, S. Lee, *et al.*, Spectrum and low-energy gap in triangular quantum spin liquid $NaYbSe_2$, arXiv:2406.17773v2.

[28] Y. Li, $YbMgGaO_4$: A triangular-lattice quantum spin liquid candidate, Adv. Quantum Technol. **2**, 1900089 (2019).

[29] J. A. Paddison, M. Daum, Z. Dun, G. Ehlers, Y. Liu, M. B. Stone, H. Zhou, and M. Mourigal, Continuous excitations of the triangular-lattice quantum spin liquid $YbMgGaO_4$, Nat. Phys. **13**, 117 (2017).

[30] A. Scheie, E. Ghioldi, J. Xing, J. Paddison, N. Sherman, M. Dupont, L. Sanjeewa, S. Lee, A. Woods, D. Abernathy, *et al.*, Proximate spin liquid and fractionalization in the triangular antiferromagnet $KYbSe_2$, Nat. Phys. **20**, 74 (2024).

[31] K. Ranjith, S. Luther, T. Reimann, B. Schmidt, P. Schlender, J. Sichelschmidt, H. Yasuoka, A. Strydom, Y. Skourski, J. Wosnitza, *et al.*, Anisotropic field-induced ordering in the triangular-lattice quantum spin liquid $NaYbSe_2$, Phys. Rev. B **100**, 224417 (2019).

[32] P.-L. Dai, G. Zhang, Y. Xie, C. Duan, Y. Gao, Z. Zhu, E. Feng, Z. Tao, C.-L. Huang, H. Cao, *et al.*, Spinon Fermi surface spin liquid in a triangular lattice antiferromagnet $NaYbSe_2$, Phys. Rev. X **11**, 021044 (2021).

[33] M. M. Bordelon, E. Kenney, C. Liu, T. Hogan, L. Posthuma, M. Kavand, Y. Lyu, M. Sherwin, N. P. Butch, C. Brown, *et al.*, Field-tunable quantum disordered ground state in the triangular-lattice antiferromagnet $NaYbO_2$, Nat. Phys. **15**, 1058 (2019).

[34] L. Ding, P. Manuel, S. Bachus, F. Grußler, P. Gegenwart, J. Singleton, R. D. Johnson, H. C. Walker, D. T. Adroja, A. D. Hillier, *et al.*, Gapless spin-liquid state in the structurally disorder-free triangular antiferromagnet $NaYbO_2$, Phys. Rev. B **100**, 144432 (2019).

[35] M. Baenitz, P. Schlender, J. Sichelschmidt, Y. Onykiienko, Z. Zangeneh, K. Ranjith, R. Sarkar, L. Hozoi, H. Walker, J.-C. Orain, *et al.*, $NaYbS_2$: A planar spin-1/2 triangular-lattice magnet and putative spin liquid, Phys. Rev. B **98**, 220409 (2018).

[36] R. Bag, S. Xu, N. E. Sherman, L. Yadav, A. I. Kolesnikov, A. A. Podlesnyak, E. S. Choi, I. Da Silva, J. E. Moore, and S. Haravifard, Evidence of Dirac quantum spin liquid in $YbZn_2GaO_5$, Phys. Rev. Lett. **133**, 266703 (2024).

[37] J. Khatua, S. Bhattacharya, A. Strydom, A. Zorko, J. Lord, A. Ozarowski, E. Kermarrec, and P. Khuntia, Magnetic properties and spin dynamics in the spin-orbit driven $J_{eff} = 1/2$ triangular lattice antiferromagnet $Ba_6Yb_2Ti_4O_{17}$, Phys. Rev. B **109**, 024427 (2024).

[38] S. Guo, A. Ghasemi, C. Broholm, and R. Cava, Magnetism on ideal triangular lattices in $NaBaYb(BO_3)_2$, Phys. Rev. Mater. **3**, 094404 (2019).

[39] T. Ferreira, J. Xing, L. D. Sanjeewa, and A. S. Sefat, Frustrated magnetism in triangular lattice $TlYbS_2$ crystals grown via molten flux, Front. Chem. **8**, 127 (2020).

[40] J. Xing, L. D. Sanjeewa, A. F. May, and A. S. Sefat, Synthesis and anisotropic magnetism in quantum spin liquid candidates $AYbSe_2$ (A = K and Rb), APL Mater. **9**, 111104 (2021).

[41] M. Xie, W. Zhuo, Y. Cai, Z. Zhang, and Q. Zhang, Rare-earth chalcogenides: An inspiring playground for exploring frustrated magnetism, Chin. Phys. Lett. **41**, 117505 (2024).

[42] Z. Zhang, X. Ma, J. Li, G. Wang, D. Adroja, T. Perring, W. Liu, F. Jin, J. Ji, Y. Wang, *et al.*, Crystalline electric field excitations in the quantum spin liquid candidate $NaYbSe_2$, Phys. Rev. B **103**, 035144 (2021).

[43] Z. Zhang, J. Li, M. Xie, W. Zhuo, D. Adroja, P. J. Baker, T. Perring, A. Zhang, F. Jin, J. Ji, *et al.*, Low-energy spin dynamics of the quantum spin liquid candidate $NaYbSe_2$, Phys. Rev. B **106**, 085115 (2022).

[44] N. Li, M. Xie, Q. Huang, Z. Zhuo, Z. Zhang, E. Choi, Y. Wang, H. Liang, Y. Sun, D. Wu, *et al.*, Thermodynamics and heat transport in the quantum spin liquid candidates $NaYbS_2$ and $NaYbSe_2$, Phys. Rev. B **110**, 224414 (2024).

[45] J. Xing, L. D. Sanjeewa, J. Kim, G. Stewart, A. Podlesnyak, and A. S. Sefat, Field-induced magnetic transition and spin fluctuations in the quantum spin-liquid candidate $CsYbSe_2$, Phys. Rev. B **100**, 220407 (2019).

[46] K. Ranjith, D. Dmytriieva, S. Khim, J. Sichelschmidt, S. Luther, D. Ehlers, H. Yasuoka, J. Wosnitza, A. A. Tsirlin, H. Kühne, *et al.*, Field-induced instability of the quantum spin

liquid ground state in the J_{eff}= 1/2 triangular-lattice compound $NaYbO_2$, Phys. Rev. B **99**, 180401 (2019).

[47] R. Sarkar, P. Schlender, V. Grinenko, E. Haeussler, P. J. Baker, T. Doert, and H.-H. Klauss, Quantum spin liquid ground state in the disorder free triangular lattice $NaYbS_2$, Phys. Rev. B **100**, 241116 (2019).

[48] T. Xie, A. Eberharter, J. Xing, S. Nishimoto, M. Brando, P. Khanenko, J. Sichelschmidt, A. Turrini, D. Mazzone, P. Naumov, *et al.*, Complete field-induced spectral response of the spin-1/2 triangular-lattice antiferromagnet $CsYbSe_2$, npj Quantum Mater. **8**, 48 (2023).

[49] T. Fujii, M. Pillaca, F. Bärtl, J. Sichelschmidt, S. Luther, H. Rosner, A. Strydom, J. Wosnitza, H. Kühne, T. Doert, *et al.*, $TlYbSe_2$ as a member of the $J = 1/2$ triangular-lattice Yb delafossite family: From spin liquid to field-induced magnetic order, Phys. Rev. B **112**, 024426 (2025).

[50] J. Alicea, O. I. Motrunich, and M. P. Fisher, Algebraic vortex liquid in spin-1/2 triangular antiferromagnets: Scenario for Cs_2CuCl_4, Phys. Rev. Lett. **95**, 247203 (2005).

[51] X.-Y. Song, C. Wang, A. Vishwanath, and Y.-C. He, Unifying description of competing orders in two-dimensional quantum magnets, Nat. Commun. **10**, 4254 (2019).

[52] J. Willsher and J. Knolle, Dynamics and stability of U(1) spin liquids beyond mean-field theory: Triangular-lattice J_2-J_2 Heisenberg model, arXiv:2503.13831.

[53] See Supplemental Material at http://link.aps.org/supplemental/10.1103/tc4h-cq9c for details of measurement methods and the phenomenological account for the linear specific heat, which includes Refs. [19,27,29,31,33,52,54–68]

[54] J. Rodríguez-Carvajal, Recent advances in magnetic structure determination by neutron powder diffraction, Physica B **192**, 55 (1993).

[55] M. Duczmal and L. Pawlak, Magnetic and structural characterization of $TlLnSe_2$ compounds (Ln Nd to Yb), J. Alloys Compd. **225**, 181 (1995).

[56] G. Hester, H. Nair, T. Reeder, D. Yahne, T. DeLazzer, L. Berges, D. Ziat, J. Neilson, A. A. Aczel, G. Sala, *et al.*, Novel strongly spin-orbit coupled quantum dimer magnet: $Yb_2Si_2O_7$, Phys. Rev. Lett. **123**, 027201 (2019).

[57] Y. Li, H. Liao, Z. Zhang, S. Li, F. Jin, L. Ling, L. Zhang, Y. Zou, L. Pi, Z. Yang, *et al.*, Gapless quantum spin liquid ground state in the two-dimensional spin-1/2 triangular antiferromagnet $YbMgGaO_4$, Sci. Rep. **5**, 16419 (2015).

[58] U. Arjun, K. M. Ranjith, A. Jesche, F. Hirschberger, D. Sarma, and P. Gegenwart, Efficient adiabatic demagnetization refrigeration to below 50 mK with ultrahigh-vacuum-compatible ytterbium diphosphates $AYbP_2O_7$ (A = Na, K), Phys. Rev. Appl. **20**, 014013 (2023).

[59] U. Arjun, K. M. Ranjith, A. Jesche, F. Hirschberger, D. D. Sarma, and P. Gegenwart, Adiabatic demagnetization refrigeration to millikelvin temperatures with the distorted square lattice magnet $NaYbGeO_4$, Phys. Rev. B **108**, 224415 (2023).

[60] M. Mitric, B. Antic, M. Balanda, D. Rodic, and M. L. Napijalo, An x-ray diffraction and magnetic susceptibility study of $Yb_xY_{2-x}O_3$, J. Phys.: Condens. Matter **9**, 4103 (1997).

[61] S. Mugiraneza and A. M. Hallas, Tutorial: A beginner's guide to interpreting magnetic susceptibility data with the Curie-Weiss law, Commun. Phys. **5**, 95 (2022).

[62] C. Kittel, *Introduction to Solid State Physics*, 6th ed. (John Wiley & Sons, Inc., New York, 1986).

[63] S. Thamban, U. Arjun, M. Padmanabhan, and R. Nath, Structural and magnetic properties of spin-1/2 dimer compound $Cu_2(IPA)_2(DMF)(H_2O)$ with a large spin gap, J. Phys.: Condens. Matter **29**, 255801 (2017).

[64] S.-S. Gong, W. Zheng, M. Lee, Y.-M. Lu, and D. N. Sheng, Chiral spin liquid with spinon Fermi surfaces in the spin-1/2 triangular Heisenberg model, Phys. Rev. B **100**, 241111 (2019).

[65] J. Nasu, M. Udagawa, and Y. Motome, Thermal fractionalization of quantum spins in a Kitaev model: Temperature-linear specific heat and coherent transport of Majorana fermions, Phys. Rev. B **92**, 115122 (2015).

[66] K. Wang, S. Feng, P. Zhu, R. Chi, H.-J. Liao, N. Trivedi, and T. Xiang, Fractionalization signatures in the dynamics of quantum spin liquids, Phys. Rev. B **111**, L100402 (2025).

[67] P. Zhu, S. Feng, K. Wang, T. Xiang, and N. Trivedi, Emergent quantum Majorana metal from a chiral spin liquid, Nat. Commun. **16**, 2420 (2025).

[68] H. Akiyama and D. Jido, Systematic study of hadronic excitation energy using the Schottky anomaly, Phys. Rev. D **104**, 114014 (2021).

[69] B. Schmidt and P. Thalmeier, Frustrated two dimensional quantum magnets, Phys. Rep. **703**, 1 (2017).

[70] R. Chen, H. Ju, H.-C. Jiang, O. A. Starykh, and L. Balents, Ground states of spin-1/2 triangular antiferromagnets in a magnetic field, Phys. Rev. B **87**, 165123 (2013).

[71] A. Honecker, J. Schulenburg, and J. Richter, Magnetization plateaus in frustrated antiferromagnetic quantum spin models, J. Phys.: Condens. Matter **16**, S749 (2004).

[72] A. Syromyatnikov, Unusual dynamics of spin-1/2 antiferromagnets on the triangular lattice in magnetic field, Ann. Phys. **454**, 169342 (2023).

[73] J. A. Mydosh, Spin glasses: Redux: An updated experimental/materials survey, Rep. Prog. Phys. **78**, 052501 (2015).

[74] J. A. Mydosh, *Spin Glasses: An Experimental Introduction* (CRC Press, London, 1993).

[75] P. Bag, P. Baral, and R. Nath, Cluster spin-glass behaviour and memory effect in $Cr_{0.5}Fe_{0.5}Ga$, Phys. Rev. B **98**, 144436 (2018).

[76] M. S. Rusanov, M. A. Kuznetsov, V. S. Zverev, and E. A. Elfimova, Influence of a bias dc field and an ac field amplitude on the dynamic susceptibility of a moderately concentrated ferrofluid, Phys. Rev. E **108**, 024607 (2023).

[77] L. Seabra, T. Momoi, P. Sindzingre, and N. Shannon, Phase diagram of the classical Heisenberg antiferromagnet on a triangular lattice in an applied magnetic field, Phys. Rev. B **84**, 214418 (2011).

[78] S. Yamashita, Y. Nakazawa, M. Oguni, Y. Oshima, H. Nojiri, Y. Shimizu, K. Miyagawa, and K. Kanoda, Thermodynamic properties of a spin-1/2 spin-liquid state in a κ-type organic salt, Nat. Phys. **4**, 459 (2008).

[79] K. Ishida, M. Morishita, K. Yawata, and H. Fukuyama, Low temperature heat-capacity anomalies in two-dimensional solid ^3He, Phys. Rev. Lett. **79**, 3451 (1997).

[80] V. Elser, Nuclear antiferromagnetism in a registered ^3He solid, Phys. Rev. Lett. **62**, 2405 (1989).

[81] R. Rawl, L. Ge, H. Agrawal, Y. Kamiya, C. Dela Cruz, N. Butch, X. Sun, M. Lee, E. Choi, J. Oitmaa, *et al.*, $Ba_8CoNb_6O_{24}$: A spin-1/2 triangular-lattice Heisenberg antiferromagnet in the two-dimensional limit, Phys. Rev. B **95**, 060412 (2017).

[82] Y. Cui, J. Dai, P. Zhou, P. Wang, T. Li, W. Song, J. Wang, L. Ma, Z. Zhang, S. Li, *et al.*, Mermin-Wagner physics, (H, T) phase diagram, and candidate quantum spin-liquid phase in the spin-1/2 triangular-lattice antiferromagnet $Ba_8CoNb_6O_{24}$, Phys. Rev. Mater. **2**, 044403 (2018).

[83] L. Chen, D.-W. Qu, H. Li, B.-B. Chen, S.-S. Gong, J. Von Delft, A. Weichselbaum, and W. Li, Two-temperature scales in the triangular-lattice Heisenberg antiferromagnet, Phys. Rev. B **99**, 140404 (2019).

[84] N. Elstner, R. Singh, and A. Young, Finite temperature properties of the spin-1/2 Heisenberg antiferromagnet on the triangular lattice, Phys. Rev. Lett. **71**, 1629 (1993).

[85] B. Bernu and G. Misguich, Specific heat and high-temperature series of lattice models: Interpolation scheme and examples on quantum spin systems in one and two dimensions, Phys. Rev. B **63**, 134409 (2001).

[86] A. Steppke, M. Brando, N. Oeschler, C. Krellner, C. Geibel, and F. Steglich, Nuclear contribution to the specific heat of $Yb(Rh_{0.93}Co_{0.07})_2Si_2$, Phys. Status Solidi B **247**, 737 (2010).

[87] A. Metavitsiadis, A. Pidatella, and W. Brenig, Thermal transport in a two-dimensional Z_2 spin liquid, Phys. Rev. B **96**, 205121 (2017).

[88] S. Feng, P. Zhu, J. Knolle, and M. Knap, Transient localization from fractionalization: Vanishingly small energy transport in gapless quantum magnets, Phys. Rev. B **114**, 034423 (2026).

[89] S. Lee, A. J. Woods, M. Lee, S. Zhang, E. S. Choi, A. Scheie, D. Tennant, J. Xing, A. Sefat, and R. Movshovich, Magnetic field-temperature phase diagram of the spin-1/2 triangular lattice antiferromagnet $KYbSe_2$, Phys. Rev. B **109**, 155129 (2024).

[90] J. M. Schliesser and B. F. Woodfield, Lattice vacancies responsible for the linear dependence of the low-temperature heat capacity of insulating materials, Phys. Rev. B **91**, 024109 (2015).

[91] C. S. Kengle, S. Thomas, R. Movshovich, S. Zhang, E. S. Choi, M. Lee, P. Rosa, and A. Scheie, Random singlet physics in the exchange-disordered two-dimensional triangular material $YbCu_{1.14}Se_2$, Phys. Rev. B **113**, 134427 (2026).

[92] Y. Lyu, L. P. Cairns, J. Rodriguez, C. Liu, K. Ng, J. Singleton, J. G. Analytis, *et al.*, Entanglement randomness and gapped itinerant carriers in a frustrated quantum magnet, Phys. Rev. X **15**, 041035 (2025).

[93] B. P. Belbase, U. Arjun, S. Feng, E. S. Choi, J. Knolle, and A. Banerjee, Source data for "Finite spinon density of states in the triangular lattice delafossite $TlYbSe_2$", Version 1.0, Data set, Zenodo, 2026, https://doi.org/10.5281/zenodo.21481296.